Graphical Abstract

Blood sodium regulation by Na,K-ATPase: Euryhaline animals' salinity adaptations described by the pump's negative feedback

Peter Ruoff

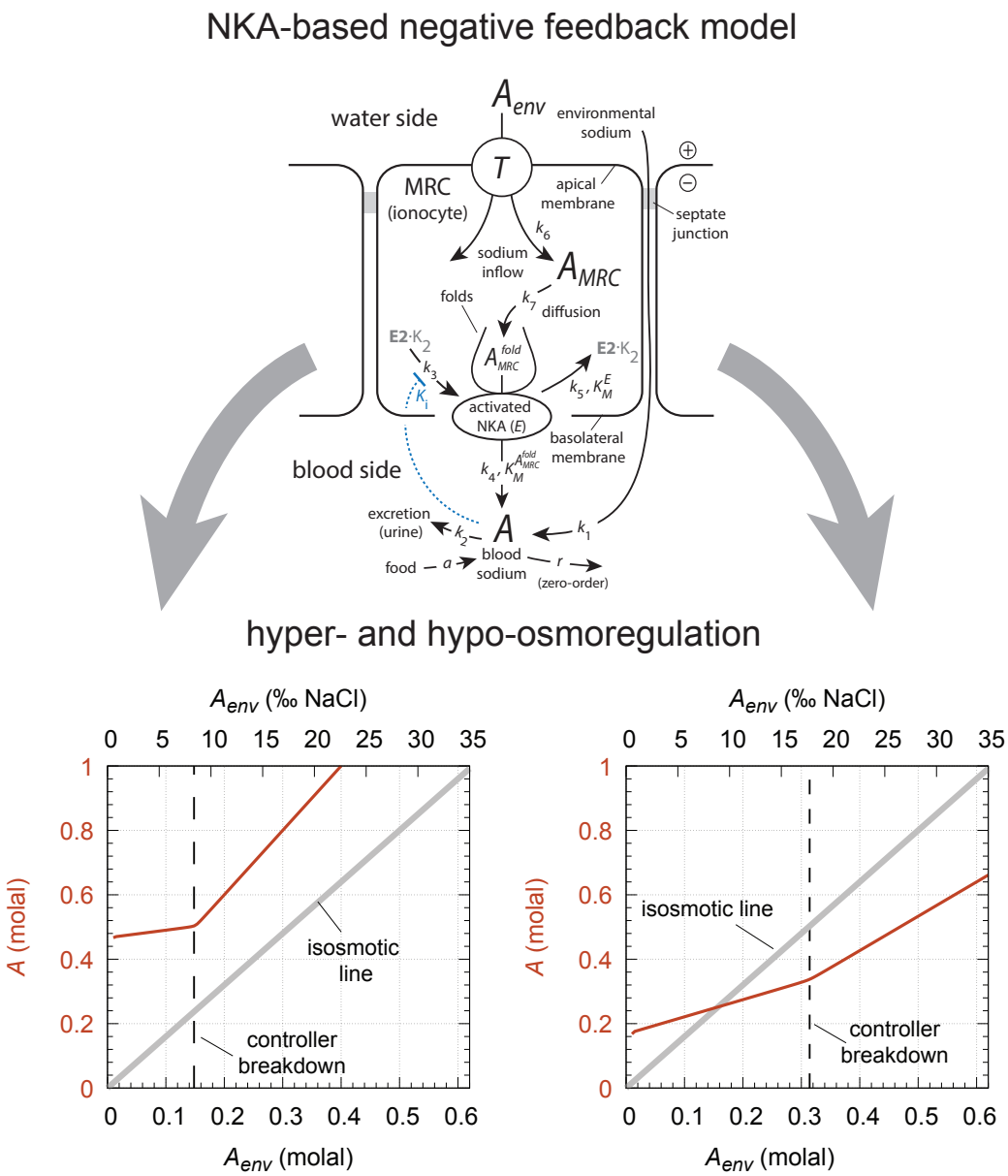

Highlights

Blood sodium regulation by Na,K-ATPase: Euryhaline animals' salinity adaptations described by the pump's negative feedback

Peter Ruoff

- Two sodium-regulating feedbacks are identified in the operation of Na,K-ATPase.
- One of these feedbacks is able to describe hypo- and hyperosmotic regulations.
- The relationship between enantiostasis and homeostasis is discussed.

Blood sodium regulation by Na,K-ATPase: Euryhaline animals' salinity adaptations described by the pump's negative feedback

Peter Ruoff

University of Stavanger, Department of Chemistry, Bioscience, and Environmental Engineering, Kjell Arholms gate 41, Stavanger, 4021, Rogaland, Norway

Abstract

The term enantiostasis was introduced by Mangum and Towle to describe a functional relationship between environmental changes and an organism's adaptation, and furthermore, to distinguish this kind of adaptation from homeostatic control. The defining example of enantiostasis is the blue crab's blood salinity adaptation when the animal is exposed to different environmental salinities during its move between the ocean and upriver locations. In this paper a model for osmoregulation is suggested based on one of two identified negative feedbacks in the mechanism of Na,K-ATPase. Using a scheme suggested by Towle in 1997 the effect of the feedback is tested with respect to the blue crab's salinity adaptation. Not only does this single feedback model give a practically quantitative description of the blue crab's adaptation data, the model is also able to show other observed patterns of osmoregulation. In view of these results the relationship between enantiostasis and homeostasis is discussed.

Keywords: Enantiostasis, homeostasis, integral control, robust perfect adaptation, Na,K-ATPase, sodium pump, dual feedback

1. Introduction: The concepts of homeostasis and enantiostasis

One of organisms' essential features is their ability to adapt to changed environmental and anticipated conditions. Homeostasis, a concept coined by Walter Cannon in 1929, is a central adaptation strategy by keeping most of an organism's steady states within relative narrow limits (Cannon, 1929; Langley, 1973; Clancy and McVicar, 2002). However, other replacing concepts

were later suggested. Mangum and Towle (1977) introduced the term *entantiostasis* to highlight an adaptation strategy with a *conserved functional relationship* between a changing environment and the organism's internal steady states (Hochachka and Somero, 1984).

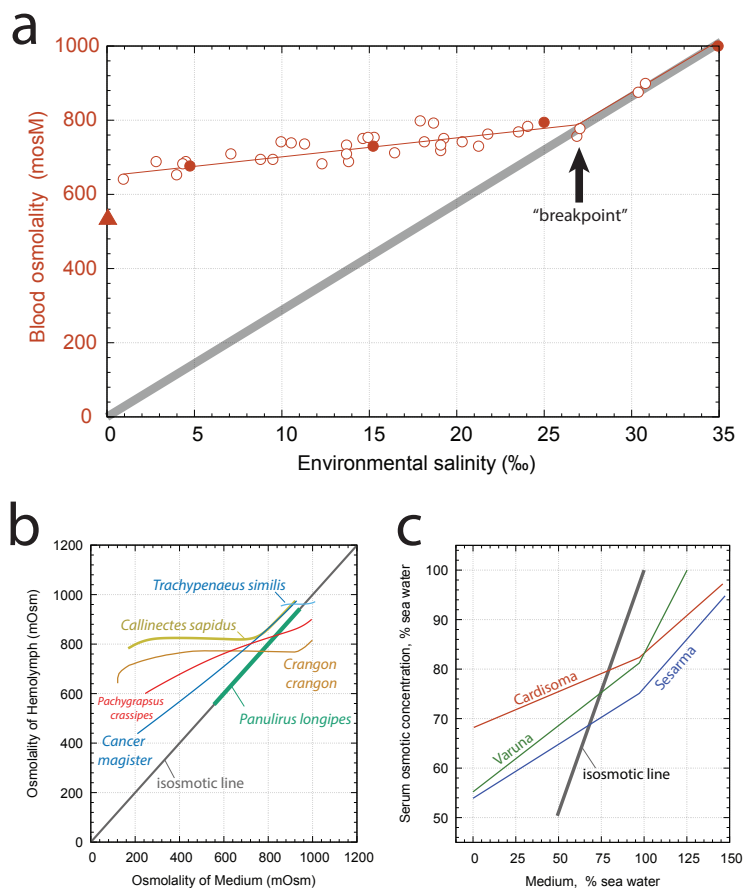

Figure 1: Types of osmoregulation. Panel a: Blood osmolality as a function of environmental salinity in the blue crab *Callinectes sapidus*. Open circles represent values of caught animals in various salinities. The triangle is the average of crabs caught in freshwater. Solid dots represent mean values of crabs acclimated at different salinities in the laboratory. The grey thick diagonal is the isosmotic line. It describes the situation when internal and environmental osmolalities are in equilibrium. Redrawn from Fig 2 of Mangum and Towle (1977). Panel b: Scheme of other hyperregulators including the osmoconformer *Panulirus longipes*. Redrawn from Figure 1 of Mantel and Farmer (1983). Panel c: Examples of hyposmotic regulators. Redrawn from Figure 1-15 of Prosser (1973).

The defining example of enantiostasis is shown in Fig 1a, which illustrates how blood osmolality in the blue crab *Callinectes sapidus* changes as the animal encounters different environmental salinities ranging from saltwater (35 ‰) to fresh water (Mangum and Towle, 1977). Since the slope in blood osmolality between 1 ‰ to about 27 ‰ is significantly greater than zero, Mangum and Towle concluded that this type of adaptation is opposite to homeostatic and termed it enantiostatic. In fact, the increased slope could also be characterized as a *rheostatic* response, a concept which was introduced by Mrosovsky (1990) focussing on setpoint changes (Stevenson, 2024), but apparently without being aware of the close similarities between these two approaches. An interesting feature in osmoregulation is the appearance of a "breakpoint" (Fig 1a), which often occurs at higher environmental salinities.

Mangum and Towle (1977) ascribed the blue crab's hyperosmotic behavior in Fig 1a (i.e. blood osmolality is higher than the osmolality of the surroundings) to a synergistic interplay between osmoregulation by Na,K-ATPase (NKA), oxygen transport, and nitrogen metabolism. The authors argued that a homeostatic, i.e. unchanged, blood salt content does not seem possible, because when crabs are moved from higher to lower water salinities the decrease in the blood's osmolality is a trigger for the production of counterions to drive the salt pump (Mangum and Towle, 1977). In addition, many studies have shown that maintaining hyperosmoregulation in crabs is accompanied by an upregulation of the sodium pump when crabs are transferred from a high salinity environment to a lower one (Towle et al., 2001). On the other hand, when testing NKA's α-subunit mRNA and protein in crabs moved from a 35 ‰ salinity to 5 ‰ no notable differences in mRNA or protein were observed. This led Towle et al. (2001) to the conclusion that the hyperosmoregulatory response in the blue crab may result from post-translational regulatory processes.

Fig 1b shows responses of other hyperosmoregulators, which differ from the blue crab both in slopes as well as where the "breakpoint" occurs. The osmoconformer *Panulirus longipes* is included, which keeps its blood osmolality at the isosmotic line where osmolalities of blood and seawater are equal. In Fig 1c examples of hyposmotic regulators are shown. These animals are normally more dilute in their body fluids than sea water and live in hypersaline lakes (Prosser, 1973).

1.1. Mechanism of NKA and dual feedback structure

NKA follows a ping-pong scheme termed as the Albers-Post mechanism (Albers, 1967; Post et al., 1969; Jorgensen et al., 2003; Dyla et al., 2020) (Fig 2a). In this scheme NKA cycles between two conformational states, $E1$ and $E2$, where potassium bound NKA in the $E2$ state binds ATP and phosphorylates the enzyme. This state releases 2 potassium ions into the internal space, thereby switching to the $E1$ conformation which binds 3 sodium ions. As pointed out by Skou and Esmann (1992) and Skou (1998), a characteristic feature of NKA is that the phosphorylation by ATP is activated by a combined effect of Na^+ on the cytoplasmic side and K^+ on the extracellular side and induces a conformation change. Skou and Esmann (1992) stress further that experiments performed on purified NKA reconstituted into liposomes show that the ATPase activity not just represents the catalytic part, but also contains the translocating part of these cations (Goldin, 1977; Cornelius and Skou, 1988). Panel b shows the dual feedback structure of the sodium pump. One of the feedbacks is based on a concentration dependent activation of NKA by internal sodium ions (Cornelius and Skou, 1988; Skou and Esmann, 1992) with the subsequent sodium expulsion by the pump (outlined in red). The other feedback occurs due to the inhibition of the pump by external sodium (Garrahan and Glynn, 1967; Sachs, 1977; Kaplan, 1982) (outlined in blue). It is the inhibitory feedback, which we will investigate.

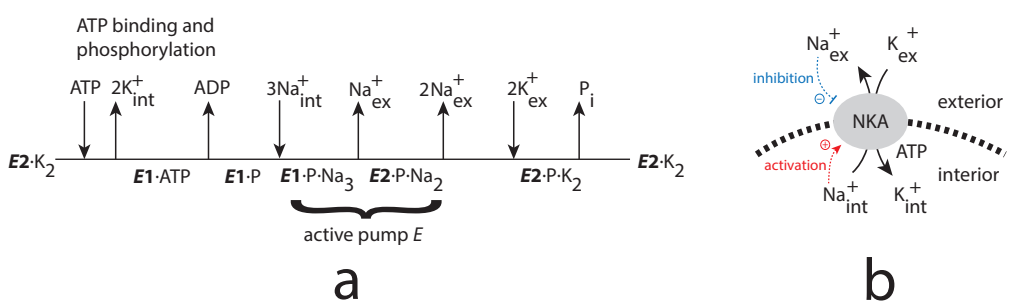

Figure 2: Mechanism of the sodium pump and the pump's dual feedback structure. Panel a: Cleland notation (Cleland, 1963) of the Albers-Post mechanism (after Jorgensen et al. (2003)). The two conformations, which pump sodium ions are indicated. Panel b: The activation of NKA by internal sodium (outlined in red) and its inhibition by external sodium (outlined in blue) create in both cases a negative feedback with respect to internal or external sodium.

2. Materials and methods

2.1. Calculations and graphical presentations

Computations were performed with the Fortran subroutine LSODE (Radhakrishnan and Hindmarsh, 1993), which can be downloaded from `https://computing.llnl.gov/projects/odepack`. Gnuplot (`www.gnuplot.info`) was used to generate figures, while reaction schemes and plot annotations were prepared with Adobe Illustrator (`www.adobe.com`). A set of Python scripts using LSODA are provided for documentation (see Supporting Material).

2.2. The model

As remarked by Mantel and Farmer (1983) the presence of up to 10% protein in the blood (hemolymph) of euryhaline animals makes a direct comparison of ionic compositions between media difficult. In the model the presence of protein and other ions is ignored by taking blood osmolality as sodium osmolality. Since sodium chloride is a dominating component in seawater the environmental salinity in Fig 1 is replaced in the model by sodium molality and ‰ NaCl. This makes model data only approximately comparable with experimental data, but still addresses the essential feature of osmoregulation by the sodium pump.

The model, shown in Fig 3, is based on the transport system described by Towle (1997) (see Fig 3 there). Instead of the three different transporters by which environmental sodium (A_{env}) enters the mitochondrial rich epithelial cells (MRCs, ionocytes), a generic transporter T is used. For simplicity, sodium enters the cytosol of the MRCs as a first-order reaction with respect to A_{env} with rate constant k_6 and velocity $v{=}k_6{\cdot}A_{env}$.

Sodium inside the MRCs, A_{MRC}, diffuses to the basolateral membrane where NKA is located (Towle and Kays, 1986). The membrane structure there shows invaginations or foldings which increase the interfacial area between blood and the basolateral membrane, and thereby increase the local NKA densities. As indicated in Fig 2b, A_{MRC} takes part in the activation of NKA leading to the $E1{\cdot}P{\cdot}Na_3$ and $E2{\cdot}P{\cdot}Na_3$ states. In the model these two states are lumped together as E (activated NKA), which moves sodium ion into the blood.

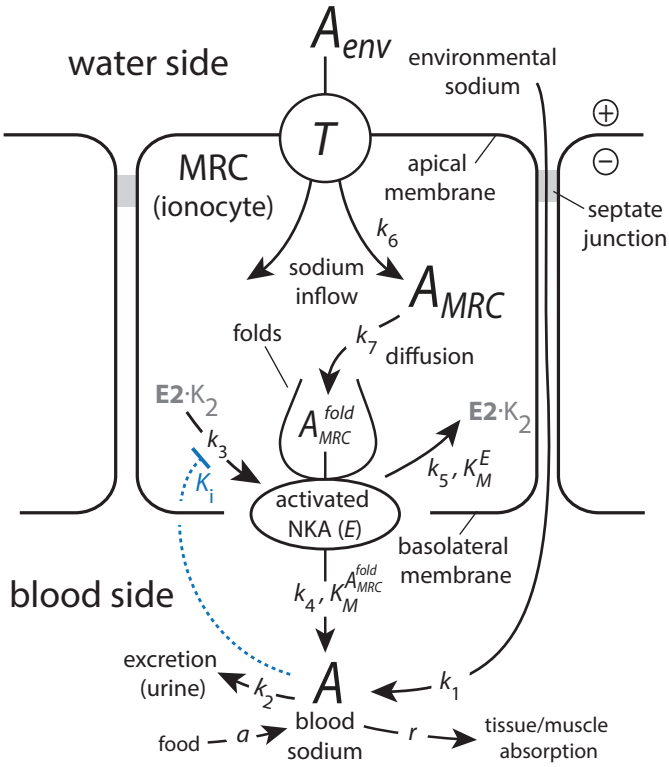

Figure 3: Negative feedback model of blood sodium homeostasis in euryhaline animals. Environmental sodium, A_{env}, enters mitochondrion rich cells (MRCs) via several transporters (Towle, 1997), lumped here together as T. Another entry route directly into the blood is considered to occur through septate junctions. Sodium ion inside MRC, A_{MRC}, diffuses to the basolateral side of the cell where NKA is situated inside a folding structure. Sodium ions located inside these folds, A^{fold}_{MRC}, are transported by activated NKA (variable E) into the blood. Activated NKA is produced from the $E2{\cdot}K_2$ state (Fig 2a) and recycled to it. The negative feedback occurs by inhibiting the activation of NKA by blood sodium (variable A) with inhibition constant K_i (outlined in blue). For rate equations, see main text.

The blood sodium concentration is described as A. Included in the model are leaky septate junctions situated between epithelial cells. Due to the apical transporters, here formulated as T, an outside-positive potential is considered to build up, which can drive a substantial inward paracellular sodium influx across the leaky junctions (Luquet et al., 2002; McNamara and Faria, 2012; Henry et al., 2012). In the model this is formulated as a first-order process with rate constant k_1. The excretion of A via the urine is described

as another first-order process with respect to A and rate constant k_2. A food-related rate a into the blood sodium pool is included in addition to a sodium storage term r which moves blood sodium into muscles and other tissues (Titze, 2015).

The rate equations are:

$$\dot{A} = k_1 \cdot A_{env} - k_2 \cdot A + \underbrace{\frac{k_4 \cdot A_{MRC}^{fold} \cdot E}{K_M^{A_{MRC}^{fold}} + A_{MRC}^{fold}}}_{compensatory\ flux\ j_4} \quad \underbrace{- \frac{r \cdot A}{K_M^r + A}}_{zero-order\ w.r.t.\ A} + a \tag{1}$$

$$\dot{E} = k_3 \cdot \underbrace{\left(\frac{K_i}{K_i + A}\right)}_{inhibition\ f_i(A)} - k_5 \cdot \underbrace{\left(\frac{E}{K_M^E + E}\right)}_{zero-order\ w.r.t.\ E} \tag{2}$$

$$\frac{d\,A_{MRC}}{dt} = k_6 \cdot A_{env} - k_7 \cdot A_{MRC} \tag{3}$$

$$\frac{d\,A_{MRC}^{fold}}{dt} = k_7 \cdot A_{MRC} - \underbrace{\frac{k_4 \cdot A_{MRC}^{fold} \cdot E}{K_M^{A_{MRC}^{fold}} + A_{MRC}^{fold}}}_{compensatory\ flux\ j_4} \tag{4}$$

2.2.1. Integral control, robust perfect adaptation, and feedback breakdown

The model has the potential to show integral control, which is a method from control engineering (Wilkie et al., 2002). Since it turns out that the model's ability to show integral control (or close to integral control) appears to be a relevant part when describing the behavior in Fig 1, the method is briefly outlined.

Integral control or integral feedback is a method from control engineering applied with respect to a negative feedback, and which requires the presence of a setpoint of a controlled variable. The difference (error ϵ) between the setpoint and the actual value of the controlled variable is calculated and integrated in time. The integrated error is then fed back into the feedback. Integral feedback leads to robust perfect adaptation (Yi et al., 2000; Khammash, 2021), where the controlled variable is moved precisely to its setpoint independent of environmental perturbations.

In chemical systems integral control can be implemented by several kinetic approaches (Yi et al., 2000; Ni et al., 2009; Drengstig et al., 2012; Shoval et al., 2010; Briat et al., 2016; Fjeld et al., 2017; Aoki et al., 2019; Waheed et al., 2022). Here, the model can show integral control in A when the second term in Eq 2 becomes close to zero-order with respect to E, i.e. when K_M^E is low in comparison with E and $E/(K_M^E{+}E)$ is close to one. At steady state, Eq 2 then defines A's setpoint at $A_{set}{=}K_i(k_3 - k_5)/k_5$, which can be seen by rearranging Eq 2:

$$\dot{E} = k_3 \cdot \underbrace{\left(\frac{K_i}{K_i{+}A}\right)}_{f_i(A)} - k_5 \cdot \underbrace{\left(\frac{E}{K_M^E{+}E}\right)}_{\approx 1} = -k_3 \underbrace{\left(\frac{k_5}{k_3} - f_i(A)\right)}_{error} \tag{5}$$

When approaching steady state the error in Eq 5 goes to zero and we get:

$$\dot{E} \to 0 \;\Rightarrow\; f_i(A) \to f_i(A_{set}) = \frac{k_5}{k_3} \;\Rightarrow\; A_{set} = \frac{K_i(k_3{-}k_5)}{k_5} \tag{6}$$

In the present feedback model the error is not a direct difference between a setpoint and the controlled variable, but between the reference value (k_5/k_3) and $f_i(A)$, as described by Eq 5. The setpoint of A is then calculated from the condition $f_i(A_{set}){=}k_5/k_3$ by solving for A_{set} (Eq 6).

3. Results

3.1. Modeling the blue crab's osmoregulation

Fig 4 shows the model's A concentration as a function of A_{env}. The experimental data by Mangum and Towle (Fig 1) are indicated as open squares. To increase A with growing A_{env} K_i is slightly increased with increasing A_{env}, i.e. in the calculations the following relationship is used:

$$K_i = K_{i,start} + \left(\frac{\Delta K_i}{\Delta A_{env}}\right) \cdot A_{env} \tag{7}$$

with

$$\frac{\Delta K_i}{\Delta A_{env}} = \frac{K_{i,end}{-}K_{i,start}}{A_{env,end}{-}A_{env,start}} \tag{8}$$

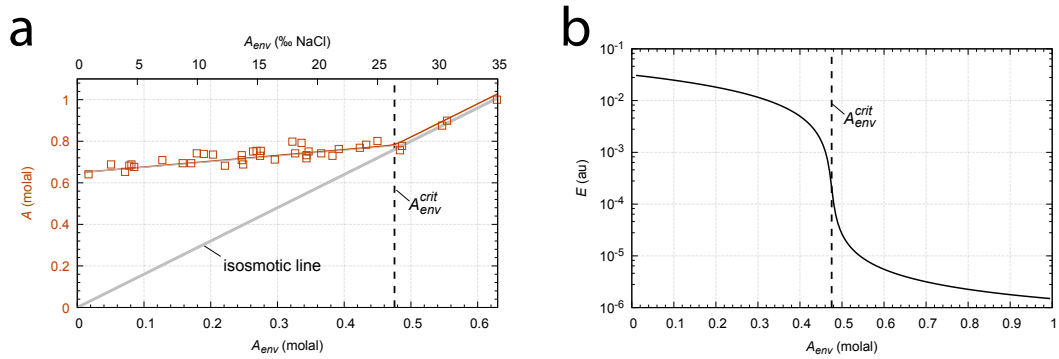

Figure 4: The blue crab's enantiostatic behavior simulated by the model (Fig 3). Panel a: Concentration of blood sodium (A) as a function of environmental sodium concentration (A_{env}). The thick grey line describes the isosmotic line. Panel b: Amount of activated NKA (E) as a function of A_{env}. The dashed vertical lines indicate A_{env}^{crit} described by Eq 11. Rate constants (au): k_1=0.16, k_2=0.1, k_3=1.0, k_4=2.0, k_5=0.1, K_M^E=1.0×10^{-6}, $K_M^{A_{MRC}^{fold}}$=1.0, k_6=100.0, k_7=1.0×10^6, a=0.022, r=0.020, K_M^r=1.0×10^{-6}. $A_{env,start}$=0.01 m and $K_{i,start}$=0.072 m, $A_{env,end}$=1.0 and $K_{i,end}$=0.103. Initial concentrations: A=0.6 m, E=0.35 au, A_{MRC}=1.0 au, A_{MRC}^{fold}=1.0 au. In the Fortran calculation the A_{env} range was divided into 200 data points. For each A_{env} value the steady state was determined after 2000 time units. See `Fig4.py` for a corresponding Python calculation.

A characteristic property of the model is that, as A_{env} increases, A homeostasis is maintained by decreasing the compensatory flux j_4 (Eq 1). Or, as crabs move towards more dilute environments blood sodium homeostasis is achieved by derepression of the pump via A, which causes an apparent increase of the pump's activity. Increased A_{env} values finally lead to a critical concentration, A_{env}^{crit}, when j_4 becomes zero and the controller breaks down. By using j_4=0 in Eq 5 the following "breakdown line" can be defined:

$$A_{ss}^{breakdown} = \frac{k_1 \cdot A_{env} + a - r}{k_2} \tag{9}$$

The intersection point between $A_{ss}^{breakdown}$ (Eq 9) and the A_{env}-dependent setpoint expression Eq 10 (which is obtained by inserting Eq 7 into Eq 6)

$$A_{set} = \left(\frac{k_3}{k_5} - 1\right)\left\{K_{i,start} + \left(\frac{\Delta K_i}{\Delta A_{env}}\right) \cdot A_{env}\right\} \tag{10}$$

determines A_{env}^{crit} as:

$$A_{env}^{crit} = \frac{K_{i,start} \cdot \left(\frac{k_3}{k_5} - 1\right) - \left(\frac{a-r}{k_2}\right)}{\left(\frac{k_1}{k_2}\right) - \left(\frac{\Delta K_i}{\Delta A_{env}}\right) \cdot \left(\frac{k_3}{k_5} - 1\right)} \tag{11}$$

As Fig 4a indicates, it is at A_{env}^{crit} the controller breakpoint in Fig 1 occurs. As A_{env} further increases the steady state values of A now follows the breakdown line Eq 9, which is different from the isosmotic line.

3.2. Robust homeostasis, controller aggressiveness, and accuracy

When K_M^E is low (zero-order conditions with respect to E, Eq 2) A_{set} depends only on k_3, k_5, and K_i. The controller shows robust perfect adaptation, and changes in the other rate constants do not affect A_{set}. This is illustrated in Fig 5 for varying k_1 and k_2 values during four phases when A_{env}=0.2 m and K_i=7.735×10^{-2} leading to a A_{set} of 0.696 m. In phase 1 k_1 and k_2 and the other rate constants have the same values as in Fig 4, while in phase 2 k_1 is doubled. In phase 3, k_1 is returned to its value during phase 1, while k_2 is trippled. Finally, in phase 4 both k_1 and k_2 are significantly reduced. Despite these changes A is kept robustly at A_{set}=0.696.

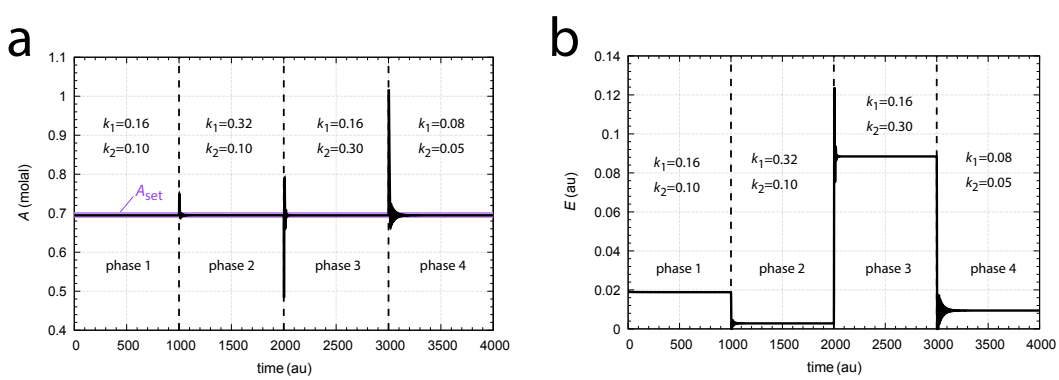

Figure 5: Perfect adaptation of A at A_{set}=0.696 (violet line) when k_1 and k_2 are changed and A_{env} is constant. Panel a: A as a function of time. Panel b: E as a function of time showing its perturbation dependent repression and derepression. A's setpoint is given by Eq 6. A_{env}=0.2 m with a K_i of 7.735×10^{-2}. The k_1, k_2 values are indicated in the figure. All other rate constants are as in Fig 4. Initial concentrations: A=0.696 m, E=0.018 au, A_{MRC}=2.0×10^{-3} au, A_{MRC}^{fold}=98.117 au. See `Fig5.py` for a corresponding Python calculation.

The term 'aggressiveness' relates to how fast a feedback responds towards a perturbation and how fast a controlled variable is moved to its setpoint. As an illustration for altered aggressiveness, k_3 and k_5 are changed by a common factor. This will influence the response kinetics of the NKA loop, but keep the setpoint of A unaffected. The violet curve in Fig 6 shows the response of A and E during two phases when at t=20 time units k_1 is changed from 0.16 (phase 1) to 0.32 (phase 2). During both phases k_3 and k_5 are kept constant at respectively 1×10^{-2} and k_5=1×10^{-3}. This results in a smooth unimodal response of A, which takes around 180 time units to reach again A_{set}=0.696 m.

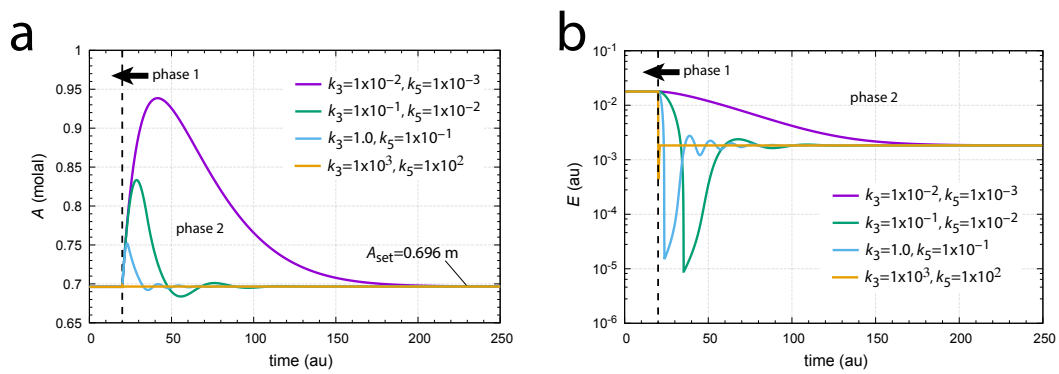

Figure 6: Illustration of NKA aggressiveness by changing k_3 and k_5 with a common factor. Panel a: Response of A to the step perturbation k_1: $0.16 \rightarrow 0.32$ applied at $t = 20$ time units using four different k_3, k_5 combinations (see insets). As k_3 and k_5 increase A's response becomes more aggressive. Panel b: The corresponding responses of E. See `Fig6.py.` for a corresponding Python script.

The green and blue lines show the effect when k_3 and k_5 are both increased by respectively one and two orders of magnitude. A's adaptation becomes significantly faster, but is also accompanied by a damped oscillatory behavior. Finally, the orange line in Fig 6a shows the response when k_3 and k_5 are increased by five orders of magnitude each. The controller has become highly aggressive with a practically instantaneous adaptation to A_{set}.

The 'accuracy' of a controller reflects its capability to adapt to the same setpoint independent of an applied perturbation. Fig 7 illustrates how K_M^E affects the NKA feedback's accuracy. We have the same perturbations as in Fig 5, but K_M^E is now increased to 1×10^{-3}. Controlled variable A no longer

adapts perfectly to its previous setpoint (violet line), but the steady state values of A have become significantly dependent on the magnitude of the perturbation.

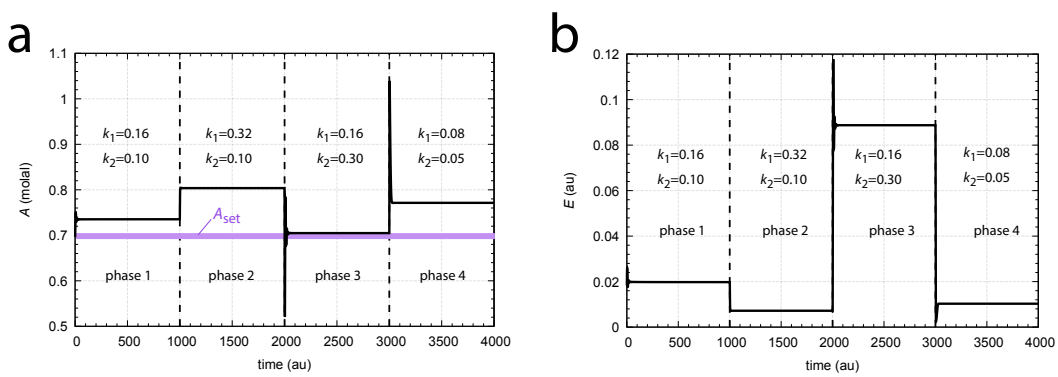

Figure 7: The accuracy of the NKA controller declines as K_M^E is increased. The system shown is the same as in Fig 5, but K_M^E is increased to 1.0×10^{-3}. A_{ss} now shows significant deviations above A_{set}, which vary with the magnitude of the perturbation. See also `Fig7.py`.

The reason for this can be seen when considering a unit inhibition ($f_i(A)$=1) in Eq 2. In this case the steady state of E is calculated as

$$E_{ss} = \left(\frac{k_3}{k_5 - k_3}\right) \cdot K_M^E \tag{12}$$

which is proportional to K_M^E. Thus, when K_M^E is increased also E_{ss} increases. This leads to larger compensatory sodium inflows into the blood compared with the situation when integral control is operative and K_M^E is much lower. Due to the increased compensatory inflow at higher K_M^E, A_{ss} values will therefore stay above A_{set}.

3.3. Other osmoregulatory schemes

Eqs 9, 10, and their resulting intersection point A_{env}^{crit} (Eq 11) determine the responses of the model, which include hyperosmotic as well as hyposmotic behaviors. This is indicated in Fig 8. Panels a and b show respective hyperosmotic and hyposmotic responses in A together with the corresponding repressions of E as A_{env} increases. The calculating procedure is the same as

described for Fig 4. The changes in K_i affect A_{set} (Eq 6) prior to NKA breakdown, while k_1, k_2, a, and r affect the $A_{ss}^{breakdown}$ slope when A_{env} exceeds A_{env}^{crit}.

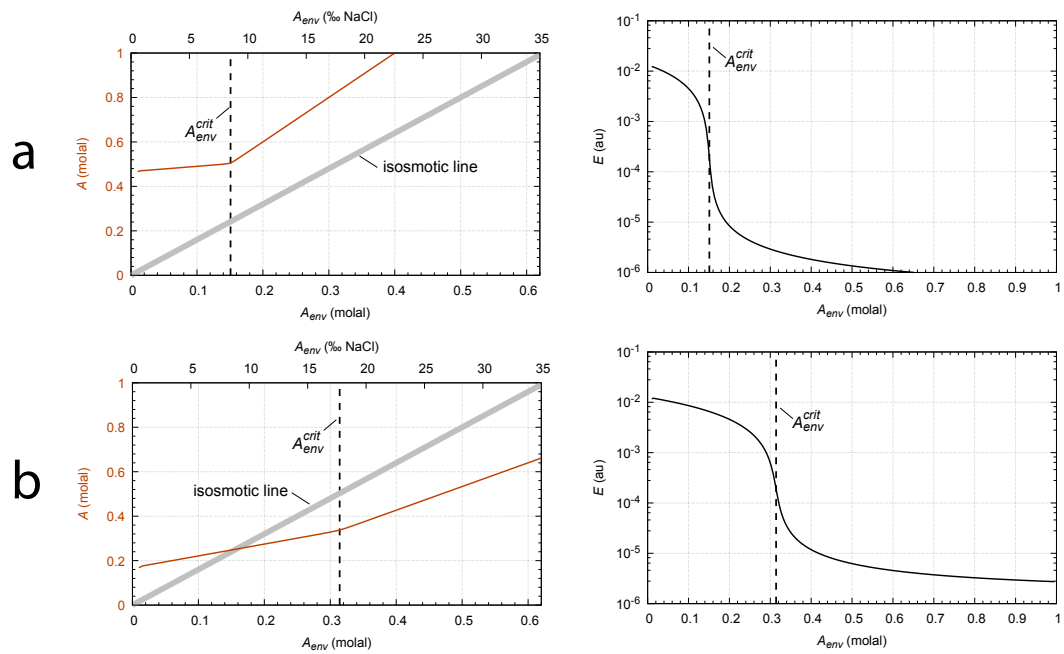

Figure 8: Hyperosmotic and hyposmotic responses of the model. Panel a: A hyperosmotic scheme where A does not cross the isosmotic line. Panel b: A hyposmotic response. A crosses the isosmotic line. Rate parameters panel a: k_1=0.2, k_2=0.1, k_3=1.0, k_4=2.0, k_5=0.3, K_M^E=1.0×10^{-6}, $K_M^{A_{MRC}^{fold}}$=1.0, k_6=100.0, k_7=1.0×10^6, a=0.03, r=0.01, K_M^r=1.0×10^{-6}. $A_{env,start}$=0.01 m and $K_{i,start}$=0.2 m, $A_{env,end}$=1.0 m and $K_{i,end}$=0.3 m. Initial concentrations, panel a: A=0.6 m, E=0.35 au, A_{MRC}=1.0 au, A_{MRC}^{fold}=1.0 au. Rate parameters panel b: k_1=0.16, k_2=0.15, k_3=1.0, k_4=2.0, k_5=0.3, K_M^E=1.0×10^{-6}, $K_M^{A_{MRC}^{fold}}$=1.0, k_6=100.0, k_7=1.0×10^6, a=r=0.03, K_M^r=1.0×10^{-6}. $A_{env,start}$=0.01 m and $K_{i,start}$=0.072 m, $A_{env,end}$=1.0 and $K_{i,end}$=0.3. Same initial concentrations as for panel a. For the Python scripts, see `Fig8a.py` and `Fig8b.py`.

4. Discussion

The term 'enantiostasis' was introduced by Mangum and Towle to distinguish the salinity adaptations of euryhaline animals from homeostatic behaviors (Mangum and Towle, 1977; Hochachka and Somero, 1984). The argument by Mangum and Towle assumed (as also done later by Mrosovsky

(1990); Stevenson (2024) when introducing the concept of 'rheostasis') that homeostasis is related to a constant setpoint in relation with a single negative feedback loop. Although Cannon's definition of homeostasis (Cannon, 1929) stressed the importance that steady states should be kept within narrow limits, Cannon didn't claim that these steady states should be constant, but are the result of coordinated actions. In fact, Cannon seemed to be well aware about how crustaceans regulate the composition of their blood in dependency to environmental salinities. In his 1929 defining homeostasis paper he cited Fredericq (1885) on this matter. See further the comment by Langley (1973) how Fredericq's work on regulation influenced Cannon's view on homeostasis.

The model presented here is based on a single negative feedback loop by inhibiting NKA in parallel with the inflow of sodium ions into the blood via septate junctions. Excretion of sodium via urine and the sodium absorption r to various tissues enable a steady state in A. To keep the model as simple as possible, additional possible sodium outflows from the blood into the seawater via septate junctions (or otherwise) (Sáez et al., 2009; McNamara and Faria, 2012) have not been included as they serve the same function as sodium excretion.

MRCs undergo significant structural changes when environmental salinities vary (Mantel and Farmer, 1983; Luquet et al., 2002). These changes within MRCs may also lead to conformational changes of NKA, and possibly affect the enzyme's rate parameters. For the sake of simplicity, it has been assumed that only K_i is affected by changed A_{env}, while allosteric effects on the other rate parameters in Eq 6 are not considered.

As indicated in Fig 2b NKA is activated by internal sodium, while external sodium inhibits the enzyme. The reader may wonder what happened with the activation of NKA in the model Fig 3. Using shark NKA, Cornelius and Skou (1988) found that the Na^+ half-maximal activation $K_{0.5}$ was found to be about 6 mM, independent of the extracellular concentration of Na^+. Thus, in the model I have simply absorbed the (assumed constant) activation term into k_3.

Concerning the inhibition constant K_i of NKA by blood sodium, Sachs (1977) found, dependent on the formulations of the model, values between 4.4 mM and 12.0 mM. In our calculations K_i varied between 0.072 m and

0.099 m.

Interestingly, NKA can act both as an inflow or outflow controller, dependent on the enzyme's transport orientation. Fig 9 gives a schematic overview. In panel a NKA acts as an outflow controller by moving the controlled species A out of the cell, while A_{env} is considered to be constant. The term r_a denotes the rate forming activated NKA*, which includes implicitly the inhibition by constant A_{env} and explicitly the activation by the controlled species A, i.e.

$$\frac{d\,(NKA^*)}{d\,t} = r_a \cdot \frac{A_{ss}}{K_a + A_{ss}} - r_d = 0 \;\;\Rightarrow\;\; A_{set} = A_{ss} = \frac{K_a \cdot r_d}{r_a - r_d} \tag{13}$$

Fig 9b shows the inflow control by NKA as in Fig 3. The term r_a now implicitly contains NKA's activation by A_{env} and explicitly the inhibition by the controlled variable A:

$$\frac{d\,(NKA^*)}{d\,t} = r_a \cdot \frac{K_i}{K_i + A_{ss}} - r_d = 0 \;\;\Rightarrow\;\; A_{set} = A_{ss} = \frac{K_i \cdot (r_a - r_d)}{r_d} \tag{14}$$

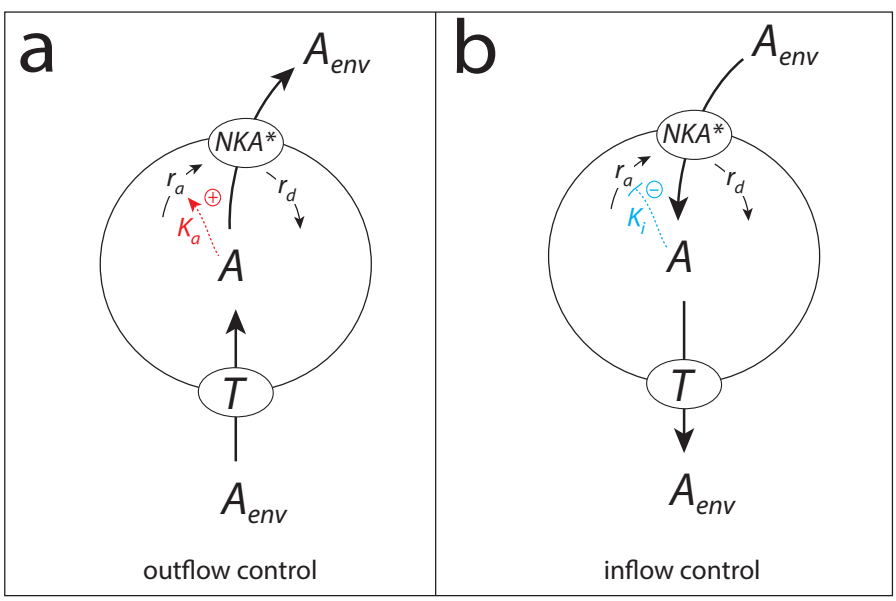

Figure 9: NKA can act as an outflow and inflow controller relative to the controlled variable A. Panel a: NKA acts as an outflow controller with an idealized integral control setpoint described by Eq 13. In panel b NKA acts as an inflow controller with setpoint described by Eq 14. NKA* represents the activated pump.

Thus, NKA may act in two ways dependent on the enzyme's flux orientation. When acting as an outflow controller with respect to the controlled variable A (Fig 9a), we have a situation as observed for red cells where NKA moves sodium from the cell into the blood (Skou, 1998). Alternatively, when NKA acts as an inflow controller, as considered in this work, A is added to maintain homeostasis (Fig 9b).

A typical problem when dealing with simulations of biochemical processes is that experimentally determined rate parameters may not be available and that parameter values (to describe a certain outcome) depend on how a model is formulated. In our case many of the parameters used in the model are not known and possibly will depend on the type of organism or tissue. Furthermore, the model also represents an idealization when considering zero-order transitions from an activated NKA to the other NKA states in the Albers-Post cycle (Fig 2a). In fact, integral control may not be ideal since K_M^E values may be larger; thus certain A_{env}-based deviations from an ideal setpoint may occur as indicated in Fig 7 and in Drengstig et al. (2012). On the other hand, the data by Mangum and Towle (Fig 1a) appear to indicate a relative robust homeostatic mechanism where A_{set} increases with increasing environmental salinity. When comparing crabs treated in the laboratory (solid dots, Fig 1a) with crabs taken in the wild (open dots) a relative robust food homeostatic mechanism appears to be present, which indicates robustness in A regulation when model parameter a is varied.

Since Mangum and Towle's introduction of enantiostasis (Mangum and Towle, 1977) several other concepts appeared as alternatives to Cannon's homeostasis concept (Pereira Jr, 2021). They include rheostasis (Mrosovsky, 1990; Stevenson, 2024) and allostasis (Sterling and Eyer, 1988; McEwen and Wingfield, 2003) to mention two of them. They are often overlapping in their definition; for example they include setpoint changes, sometimes with the claim (Stevenson, 2024) that such changes cannot be explained by homeostatic mechanisms. As shown by the results from Figs 4 and 5 setpoint changes can indeed occur without compromising robust regulations. In this respect, behaviors addressed by enantiostasis or rheostasis, although important by their descriptions, appear to be emergent results of homeostatic regulation, either by single or multiple feedback loops.

Glossary

Controlled variable: The variable (here blood sodium A) which is under homeostatic control with one or several local setpoints.

Controller breakdown: Controller breakdown occurs when the compensatory flux is insufficient, as for example when j_4 (Eq 1) goes to zero.

Controller variable or manipulated variable: The controller or manipulated variable generates a compensatory flux to oppose a perturbation applied to the controlled variable. In the NKA model this is the activated NKA variable E.

Hyperosmosis: Osmolality of the blood is higher than the surrounding seawater.

Hyposmosis: Osmolality of the blood is lower than the surrounding seawater.

Integral control: In integral control the error between the controlled variable (or a function of it) and a local setpoint/reference is integrated and used as part of the negative feedback (see Eq 5). Integral control, when operative, ensures robust perfect adaptation to its setpoint when step perturbations are applied (see Fig 5).

Isosmotic line: The condition when osmolalities of blood and seawater are equal.

NKA: Na-K ATPase, sodium pump.

Supporting Material

`Python.zip`: Python codes showing the results of Figs 4, 5, 6, 7, and 8. Besides Python (`https://www.python.org`), Numpy (`https://numpy.org`), Matplotlib (`https://matplotlib.org`), and Scipy (`https://scipy.org`) need to be installed. The scripts can be run via the Terminal (Linux, Unix, Mac OSX) or the Command Prompt (Windows) by using the command '`python name.py`', where '`name`' is the name of the Python file.

Funding sources

This research did not receive any specific grant from funding agencies in the public, commercial, or not-for-profit sectors.

References

Albers, R., 1967. Biochemical aspects of active transport. Annual Review of Biochemistry 36, 727–756.

Aoki, S.K., Lillacci, G., Gupta, A., Baumschlager, A., Schweingruber, D., Khammash, M., 2019. A universal biomolecular integral feedback controller for robust perfect adaptation. Nature 570, 533–537.

Briat, C., Gupta, A., Khammash, M., 2016. Antithetic integral feedback ensures robust perfect adaptation in noisy biomolecular networks. Cell Systems 2, 15–26.

Cannon, W., 1929. Organization for Physiological Homeostasis. Physiol. Rev. 9, 399–431.

Clancy, J., McVicar, A.J., 2002. Physiology and Anatomy. A Homeostatic Approach. Second edition. Hodder Arnold Publication, London, UK.

Cleland, W., 1963. The kinetics of enzyme-catalyzed reactions with two or more substrates or products: I. Nomenclature and rate equations. Biochimica et Biophysica Acta (BBA)-Specialized Section on Enzymological Subjects 67, 104–137.

Cornelius, F., Skou, J.C., 1988. The sided action of Na^+ on reconstituted shark Na^+/K+-atpase engaged in Na^+-Na^+ exchange accompanied by atp hydrolysis. ii. transmembrane allosteric effects on Na^+ affinity. Biochimica et Biophysica Acta (BBA)-Biomembranes 944, 223–232.

Drengstig, T., Jolma, I., Ni, X., Thorsen, K., Xu, X., Ruoff, P., 2012. A Basic Set of Homeostatic Controller Motifs. Biophys J 103, 2000–2010.

Drengstig, T., Ni, X., Thorsen, K., Jolma, I., Ruoff, P., 2012. Robust adaptation and homeostasis by autocatalysis. J Phys Chem B 116, 5355–5363.

Dyla, M., Kjærgaard, M., Poulsen, H., Nissen, P., 2020. Structure and mechanism of P-type ATPase ion pumps. Annual Review of Biochemistry 89, 583–603.

Fjeld, G., Thorsen, K., Drengstig, T., Ruoff, P., 2017. Performance of homeostatic controller motifs dealing with perturbations of rapid growth and depletion. J Phys Chem B 121, 6097–6107.

Fredericq, L., 1885. The influence of the environment on the composition of blood of aquatic animals. Arch Zool Exper Gen 3, 34–8.

Garrahan, P., Glynn, I., 1967. The sensitivity of the sodium pump to external sodium. The Journal of Physiology 192, 175–188.

Goldin, S., 1977. Active transport of sodium and potassium ions by the sodium and potassium ion-activated adenosine triphosphatase from renal medulla. reconstitution of the purified enzyme into a well defined in vitro transport system. The Journal of Biological Chemistry 252, 5630–5642.

Henry, R.P., Lucu, Č., Onken, H., Weihrauch, D., 2012. Multiple functions of the crustacean gill: osmotic/ionic regulation, acid-base balance, ammonia excretion, and bioaccumulation of toxic metals. Frontiers in Physiology. Sec. Aquatic Physiology 3, 431.

Hochachka, P.W., Somero, G.N., 1984. Biochemical Adaptation. Princeton University Press, Princeton, New Jersey.

Jorgensen, P.L., Håkansson, K.O., Karlish, S.J., 2003. Structure and mechanism of Na,K-ATPase: Functional sites and their interactions. Annual Review of Physiology 65, 817–849.

Kaplan, J.H., 1982. Sodium pump-mediated ATP: ADP exchange. The sided effects of sodium and potassium ions. The Journal of General Physiology 80, 915–937.

Khammash, M.H., 2021. Perfect adaptation in biology. Cell Systems 12, 509–521.

Langley, L.L., 1973. Homeostasis. Origins of the Concept. Dowden, Hutchinson & Ross, Inc., Stroudsbourg, Pennsylvania.

Luquet, C., Genovese, G., Rosa, G., Pellerano, G., 2002. Ultrastructural changes in the gill epithelium of the crab *Chasmagnathus granulatus* (Decapoda: Grapsidae) in diluted and concentrated seawater. Marine Biology 141, 753–760.

Mangum, C., Towle, D., 1977. Physiological Adaptation to Unstable Environments: Inconstancy of the internal milieu in an animal may be a regulatory mechanism. American Scientist 65, 67–75.

Mantel, L.H., Farmer, L.L., 1983. Osmotic and Ionic Regulation, in: Bliss, Dorothy E (Ed.), The Biology of Crustacea. Volume 5: Internal Anatomy and Physiological Regulation. Academic Press, pp. 53–161.

McEwen, B.S., Wingfield, J.C., 2003. The concept of allostasis in biology and biomedicine. Hormones and Behavior 43, 2–15.

McNamara, J.C., Faria, S.C., 2012. Evolution of osmoregulatory patterns and gill ion transport mechanisms in the decapod crustacea: a review. Journal of Comparative Physiology B 182, 997–1014.

Mrosovsky, N., 1990. Rheostasis. The Physiology of Change. Oxford University Press, New York.

Ni, X., Drengstig, T., Ruoff, P., 2009. The control of the controller: Molecular mechanisms for robust perfect adaptation and temperature compensation. Biophys J 97, 1244–53.

Pereira Jr, A., 2021. Developing the concepts of homeostasis, homeorhesis, allostasis, elasticity, flexibility and plasticity of brain function. NeuroSci 2, 372–382.

Post, R., Kume, S., Tobin, T., Orcutt, B., Sen, A., 1969. Flexibility of an active center in sodium-plus-potassium adenosine triphosphatase. The Journal of General Physiology 54, 306–326.

Prosser, C.L., 1973. Water: Osmotic Balance; Hormonal Regulation, in: Prosser, C Ladd (Ed.), Comparative Animal Physiology. W. B. Saunders Company, pp. 1–78.

Radhakrishnan, K., Hindmarsh, A., 1993. Description and Use of LSODE, the Livermore Solver for Ordinary Differential Equations. NASA Reference Publication 1327, Lawrence Livermore National Laboratory Report UCRL-ID-113855. National Aeronautics and Space Administration, Lewis Research Center, Cleveland, OH 44135-3191.

Sachs, J., 1977. Kinetics of the inhibition of the Na-K pump by external sodium. The Journal of Physiology 264, 449–470.

Sáez, A.G., Lozano, E., Zaldívar-Riverón, A., 2009. Evolutionary history of Na,K-ATPases and their osmoregulatory role. Genetica 136, 479–490.

Shoval, O., Goentoro, L., Hart, Y., Mayo, A., Sontag, E., Alon, U., 2010. Fold-change detection and scalar symmetry of sensory input fields. PNAS 107, 15995–16000.

Skou, J.C., 1998. The identification of the sodium pump. Bioscience Reports 18, 155–169.

Skou, J.C., Esmann, M., 1992. The Na,K-ATPase. Journal of Bioenergetics and Biomembranes 24, 249–261.

Sterling, P., Eyer, J., 1988. Allostasis: A new paradigm to explain arousal pathology, in: Fisher, S. and Reason, J. (Ed.), Handbook of Life Stress, Cognition and Health. John Wiley & Sons, New York, pp. 629–49.

Stevenson, T.J., 2024. On Rheostasis. The Hierarchical Organization of Physiological Stability. Oxford University Press, New York.

Titze, J., 2015. A different view on sodium balance. Current Opinion in Nephrology and Hypertension 24, 14–20.

Towle, D.W., 1997. Molecular approaches to understanding salinity adaptation of estuarine animals. American Zoologist 37, 575–584.

Towle, D.W., Kays, W.T., 1986. Basolateral localization of Na^++ K^+-ATPase in gill epithelium of two osmoregulating crabs, *Callinectes sapidus* and *Carcinus maenas*. Journal of Experimental Zoology 239, 311–318.

Towle, D.W., Paulsen, R.S., Weihrauch, D., Kordylewski, M., Salvador, C., Lignot, J.H., Spanings-Pierrot, C., 2001. Na^++ K^+-ATPase in gills of the

blue crab *Callinectes sapidus*: cDNA sequencing and salinity-related expression of α-subunit mRNA and protein. Journal of Experimental Biology 204, 4005–4012.

Waheed, Q., Zhou, H., Ruoff, P., 2022. Kinetics and mechanisms of catalyzed dual-E (antithetic) controllers. PLoS One 17, e0262371.

Wilkie, J., Johnson, M., Reza, K., 2002. Control Engineering. An Introductory Course. Palgrave, New York.

Yi, T., Huang, Y., Simon, M., Doyle, J., 2000. Robust perfect adaptation in bacterial chemotaxis through integral feedback control. PNAS 97, 4649–53.